Calculated Internal Stress Distributions in Melt-Spun Fibers

WILLIAM P. BELL* and DAN D. EDIE†, *Department of Chemical Engineering, Clemson University, Clemson, South Carolina 29631*

Synopsis

Although melt spinning is a basic process in the synthetic fiber industry, theoretical understanding of heat transfer and stress development in a melt-spun fiber is limited. In this work, the finite-element method is first applied to the melt-spinning process to determine radial and axial temperature distributions in a solidfying fiber. A thermal stress analysis is then made, again by the finite-element method. Calculated stresses are found to reach maximum values shortly after the fiber solidifies. Because material properties are reduced at these elevated temperatures, this is a location of potential mechanical failure. Anisotropy due to drawing may add to this problem. Analysis of the effects of spinning parameters shows that ambient air temperature is the most critical variable in controlling the internal stresses. Mass flow rate and take-up speed have smaller effects.

INTRODUCTION

Melt spinning is a basic process in the glass and synthetic fiber industries. As shown in Figure 1, the process involves extrusion of molten polymer or glass through capillaries to form fibers. As it is extruded, the fiber is cooled from the extrusion temperature to a temperature below the material's solidification point. The fiber is simultaneously drawn, causing a decrease in its diameter. In some applications, cooling air is blown perpendicular to the fiber to enhance cooling. After collection on a winder, the fiber is usually processed further to develop desired properties.

Heat transfer from the fiber to the surrounding quench medium is important in determining the properties of the resulting fiber. This process determines the temperature and thermal stress distributions within the fiber. Internal stresses are known to have effects on fiber properties such as elastic modulus and ultimate strength and can cause cracking on the surface of the fiber.[1]

The purpose of this work is to develop a mathematical model for calculating the thermal stresses induced during the melt spinning of fibers from amorphous materials. Because thermal stresses are directly related to the temperature gradients within the fiber, the first part of this model must be the calculation of the temperature profiles in the fiber. With this information, the model may then deal with stress development as a separate problem. Experimental verification of the model is considered in a subsequent article.

*Present address: Tennessee Eastman Company, Kingsport, Tennessee
†To whom correspondence should be addressed.

Journal of Applied Polymer Science, Vol. 33, 1073–1088 (1987)
 CCC 0021-8995/87/041073-16$04.00

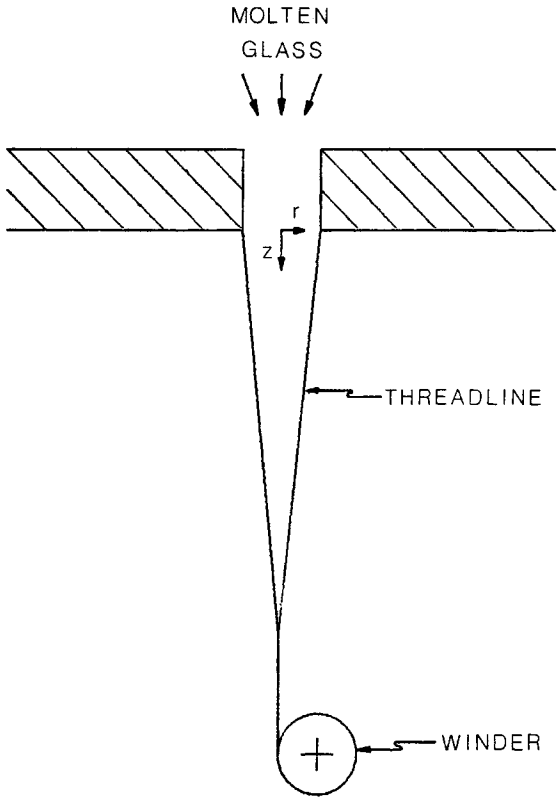

Fig. 1. Diagram of melt-spinning process.

TEMPERATURE CALCULATIONS

Numerous mathematical models have been presented for calculating temperature distributions during the melt-spinning process.[2] Of these, only three consider variation of temperature across the fiber radius. Andrews[3] reports a simplified analytical solution for an axisymmetric temperature profile for a fiber with a known shape. Matsuo and Kase[4] extend their earlier work[5] to calculate the nonaxisymmetric temperature distribution in a fiber cooled by cross-flowing air. This model uses a modified finite-difference technique and requires a prior knowledge of the fiber shape.

In the third model, Hutchenson, Edie, and Riggs[6] develop a finite-difference solution to the melt-spinning heat transfer problem. As in the Matsuo and Kase[4] model, this model assumes that radial temperature variation in the fiber has no effect on the fiber drawdown. Thus the simple model of Kase and Matsuo[5] can be used to predict the fiber radius profile. This is done by solving the simplified equations of continuity, motion, and energy:

$$\frac{dT}{dz} = -\frac{2(\pi A^*)^{0.5} h(T - T_a)}{WC_p} \tag{1}$$

$$\frac{dA^*}{dz} = -\frac{F\rho}{W\beta} A^* \tag{2}$$

where the heat transfer coefficient is given by

$$h = 0.21k_o\left(\frac{\pi}{A^*}\right)^{0.5}\left[\frac{2W}{(\pi A^*)^{0.5}\rho v_o}\right]^{0.334}(1 + C). \tag{3}$$

Here, C is a coefficient which corrects for the direction of the cooling air flow. Since the fiber shape is known, the equation of energy is decoupled from the equation of motion.

Assuming (a) steady-state spinning, (b) constant physical properties ρ, C_p, and k, (c) negligible viscous heat dissipation, (d) axisymmetric flow, (e) axisymmetric temperature distribution, and (f) negligible axial heat conduction, the equations of continuity and energy can be reduced to

$$\frac{1}{r}\frac{\partial}{\partial r}(rv_r) + \frac{\partial}{\partial z}(v_z) = 0 \tag{4}$$

$$\rho C_p\left[v_r\frac{\partial T}{\partial r} + v_z\frac{\partial T}{\partial z}\right] = k\left[\frac{1}{r}\frac{\partial}{\partial r}\left(r\frac{\partial T}{\partial r}\right)\right]. \tag{5}$$

Note that this results in a problem in two rather than three dimensions. Integrating Eq. (4) and substituting the mass flow rate W changes Eq. (5) to

$$\frac{WC_p}{\pi R^2}\left[\frac{r}{R}\frac{dR}{dz}\frac{\partial T}{\partial r} + \frac{\partial T}{\partial z}\right] = k\left[\frac{\partial^2 T}{\partial r^2} + \frac{1}{r}\frac{\partial T}{\partial r}\right] \tag{6}$$

as the governing differential equation for heat transfer in the fiber.

Hutchenson then expresses Eq. (6) in terms of dimensionless variables defined as follows:

$$\xi = \frac{r}{R(z)} \tag{7}$$

$$\zeta = \frac{\pi kz}{WC_p} \tag{8}$$

$$\theta = \frac{T - T_a}{T_{\text{spin}} - T_a}. \tag{9}$$

Substituting these three relationships into Eq. (6) reduces the governing equation to

$$\frac{\partial\theta}{\partial\zeta} = \frac{\partial^2\theta}{\partial\xi^2} + \frac{1}{\xi}\frac{\partial\theta}{\partial\xi}. \tag{10}$$

Note that in this derivation, the radial convection term cancels with one of the radial conduction terms, giving a much simpler equation.

The following boundary conditions are applied to Eq. (10).

1. The temperature at the spinneret is constant at the spinning temperature. In terms of the dimensionless variables, this is stated as

$$\theta(\xi, 0) = 1.0. \tag{11}$$

2. The radial temperature gradient is zero at the center of the fiber, or

$$\frac{\partial}{\partial \xi}\theta(0, \zeta) = 0.0. \tag{12}$$

3. Heat loss from the surface occurs by convection only. This is stated mathematically as

$$\frac{\partial}{\partial r}T(R, z) = -\frac{h}{k}(T(R, z) - T_a) \tag{13}$$

or, in dimensionless variables,

$$\frac{\partial}{\partial \xi}\theta(1, \zeta) = -\left(\frac{hR}{k}\right)\theta(1, \zeta). \tag{14}$$

The heat transfer coefficient h in Eq. (3) is used in this model.

At this point, Hutchenson applies the finite-difference method to the problem. This yields a system of linear difference equations which can be solved for the radial and axial temperature profiles in the fiber.

In the present work, the same mathematical model is used to describe the heat transfer in the melt-spinning process. However, the finite-element method is used as the solution technique, rather than the finite-difference method. The finite-element method is required in the stress calculations to follow, and convenience dictates its use for the temperature calculations also.

APPLICATION OF GALERKIN'S METHOD

To apply the finite-element method to Eq. (10), the fiber is first divided into a number of elements, as sketched in Figure 2. In this case, linear triangular elements are used, although more complex elements could be employed. Within each element, the nodes are labeled i, j, and k in a counterclockwise manner. Shape function N_β are defined such that the dimensionless temperature approximation in the element is given by

$$\tilde{\theta} = \left[N_i N_j N_k\right]\left[\theta_i \theta_j \theta_k\right]^T \tag{15}$$

where the θ_β are the reduced temperatures at the nodes.[7]

Galerkin's method states that the solution to a differential equation is best approximated when the error function is orthogonal to the weighting or shape

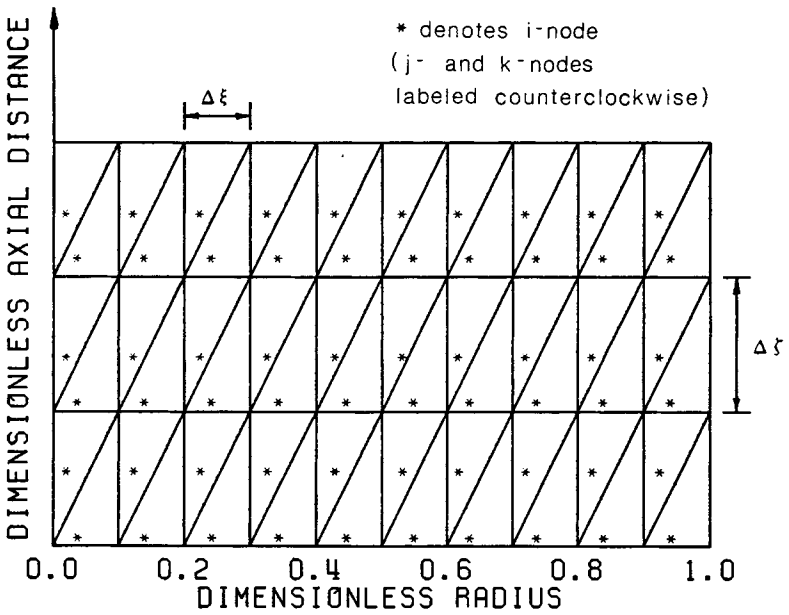

Fig. 2. Finite-element discretization of region for heat transfer problem.

functions.[7] Thus, for Eq. (10), this requirement becomes

$$\int_V [N]^T \left(\xi \frac{\partial^2 \bar{\theta}}{\partial \xi^2} + \frac{\partial \bar{\theta}}{\partial \xi} - \xi \frac{\partial \bar{\theta}}{\partial \zeta} \right) dV = 0.0 \tag{16}$$

where V refers to the volume of the fiber. Applying Green's theorem to the second derivative term in Eq. (16) gives

$$\int_V \frac{\partial}{\partial \xi} (\xi [N]^T) \frac{\partial \bar{\theta}}{\partial \xi} \, dV - \int_V [N]^T \frac{\partial \bar{\theta}}{\partial \xi} \, dV + \int_V \xi [N]^T \frac{\partial \bar{\theta}}{\partial \zeta} \, dV = \int_S \xi [N]^T \frac{\partial \bar{\theta}}{\partial \xi} \, dS \tag{17}$$

where S refers to the surface of the fiber. Chain differentiating and substituting Eq. (14) further reduces Eq. (17) to

$$\int_V \frac{\partial}{\partial \xi} [N]^T \frac{\partial \bar{\theta}}{\partial \xi} \, dV + \int_V [N]^T \frac{\partial \bar{\theta}}{\partial \zeta} \, dV = - \int_S \frac{hR}{k} [N]^T \bar{\theta} \, dS. \tag{18}$$

In this derivation, the value of ξ is assumed to be constant within an element at the centroidal value $\bar{\xi}$. Equation (15) may be substituted into Eq. (18) to give

$$\int_V \frac{\partial}{\partial \xi} [N]^T \frac{\partial}{\partial \xi} [N] \{\theta\} \, dV + \int_V [N]^T \frac{\partial}{\partial \zeta} [N] \{\theta\} \, dV$$

$$= - \int_S \frac{hR}{k} [N]^T [N] \{\theta\} \, dS. \tag{19}$$

If convection is assumed to occur only from the $j - k$ side of an element, the integrations in Eq. (19) can be performed by the area coordinate method, as described by Segerlind,[7] to yield the following set of equations for an element.

$$[k^{(e)}]\{\theta\} = \{0\} \tag{20}$$

where

$$[k^{(e)}] = \frac{\bar{\xi}}{2A}\begin{bmatrix} b_i^2 & b_ib_j & b_ib_k \\ b_ib_j & b_j^2 & b_jb_k \\ b_ib_k & b_jb_k & b_k^2 \end{bmatrix} + \frac{\bar{\xi}}{3}\begin{bmatrix} c_i & c_j & c_k \\ c_i & c_j & c_k \\ c_i & c_j & c_k \end{bmatrix} + \frac{hRL_{jk}}{3k}\begin{bmatrix} 0 & 0 & 0 \\ 0 & 2 & 1 \\ 0 & 1 & 2 \end{bmatrix} \tag{21}$$

and $\{0\}$ is the zero vector. Note that if an element does not have a side from which convective heat transfer occurs, then the third term in Eq. (21) must be dropped.

Now the element conduction matrix $[k^{(e)}]$ can be calculated for each element in the fiber and then the global conduction matrix $[K]$ can be found by proper summation of the element matrices, as per Segerlind.[7] The boundary condition in Eq. (11) is then applied by direct substitution, yielding the following final system of equations which can be solved for the values of the temperatures at the nodes.

$$[K]\{\theta\} = \sum_{\substack{\text{all} \\ \text{elements}}} [k^{(e)}]\{\theta\} = \{F\}. \tag{22}$$

Note that the zero-gradient boundary condition of Eq. (12) is an implicit assumption of the finite-element method.

STRESS CALCULATIONS

Given the temperature distribution and the axial stress applied to the fiber by the winder, the stress state within the fiber can be predicted. However, the occurrence of a phase change within the fiber complicates the problem. Various methods have been proposed for calculating these stresses. Gorissen[8] presents a numerical integration procedure for thermal stress calculation for an elastic, isotropic material with temperature-independent mechanical properties. The method gives good qualitative results, but is limited in its applicability. Lewis and Bass[9] apply the finite-element method to stress calculations for various phase change processes. The flexibility of the method allows for variable physical and mechanical properties and gives good results. In a similar paper, Rigdahl[10] reports a finite-element solution for stresses in an injection-molded polymer article.

Because it can handle the temperature dependence of physical and mechanical properties, the finite-element method was selected for the stress calculations in this work. In a stress analysis problem, the radial and axial displacements at each node are calculated so that the total potential energy of the system is minimized.[7] Once the displacements are known, the strains and stresses can be determined.

As in the heat transfer problem, the displacements in a single linear triangular element are represented by

$$\{u\} = [N^*]\{U\} \tag{23}$$

where

$$\{u\} = [u_r u_z]^T \tag{24}$$

$$[N^*] = \begin{bmatrix} N_i & 0 & N_j & 0 & N_k & 0 \\ 0 & N_i & 0 & N_j & 0 & N_k \end{bmatrix} \tag{25}$$

and

$$\{U\} = [U_{r,i} U_{z,i} U_{r,j} U_{z,j} U_{r,k} U_{z,k}]^T. \tag{26}$$

Note that in this problem there are two unknowns at each node. Mathematically minimizing the potential energy results in a set of element equations given by

$$[k^{(e)}]\{U\} = \{f^{(e)}\} \tag{27}$$

where

$$[k^{(e)}] = \int_V [B]^T [D][B]\, dV \tag{28}$$

and

$$\{f^{(e)}\} = \int_V [B]^T [D]\{\epsilon_0\}\, dV + \int_S [N]^T \{p\}\, dS. \tag{29}$$

For an axisymmetric problem such as this, the above matrices are defined as follows:

$$[B] = \frac{1}{2A} \begin{bmatrix} b_i & 0 & b_j & 0 & b_k & 0 \\ 0 & c_i & 0 & c_j & 0 & c_k \\ \dfrac{2AN_i}{r} & 0 & \dfrac{2AN_j}{r} & 0 & \dfrac{2AN_k}{r} & 0 \\ c_i & b_i & c_j & b_j & c_k & b_k \end{bmatrix} \tag{30}$$

$$[D] = \frac{E(1-\mu)}{(1+\mu)(1-2\mu)} \begin{bmatrix} 1 & \dfrac{\mu}{1-\mu} & \dfrac{\mu}{1-\mu} & 0 \\ \dfrac{\mu}{1-\mu} & 1 & \dfrac{\mu}{1-\mu} & 0 \\ \dfrac{\mu}{1-\mu} & \dfrac{\mu}{1-\mu} & 1 & 0 \\ 0 & 0 & 0 & \dfrac{1-2\mu}{2(1-\mu)} \end{bmatrix} \tag{31}$$

$$\{\epsilon_0\} = \alpha \Delta T [1\ 1\ 1\ 0]^T \tag{32}$$

$$\{p\} = [p_r p_z]^T. \tag{33}$$

Problems obviously occur in the evaluation of the integrals in Eqs. (28) and (29) because r and the shape functions vary within an element. To simplify the integrations, these variables are assumed to be constant at their centroidal values ($\bar{r}$ and $\overline{N}_\beta = \frac{1}{3}$). With this assumption, the element stiffness matrix $[k^{(e)}]$ can be evaluated directly. If the temperature of the element is taken as the average of the three nodal temperatures, the first term in Eq. (29) can be similarly evaluated. The second term in Eq. (29) can be evaluated by the area coordinate method.[7] Note that for the fiber-spinning problem, p_r is zero and p_z is the applied winder stress. The final results of the integrations follow:

$$[k^{(e)}] = 2\pi\bar{r}A[\overline{B}]^T[D][\overline{B}] \tag{34}$$

$$\{f^{(e)}\} = 2\pi\bar{r}A\alpha\Delta T[\overline{B}]^T[D]\begin{Bmatrix}1\\1\\1\\0\end{Bmatrix} + \frac{\pi L_{ij}p_z}{3}\begin{Bmatrix}0\\2R_i + R_j\\0\\R_i + 2R_j\\0\\0\end{Bmatrix} \tag{35}$$

Note that the second term in Eq. (35) is included only for those elements on the lower end of the fiber where the winder stress is applied. As in the temperature problem, the global problem is created by proper summation of the element equations.[7]

From the geometry of the problem, it may be seen that two boundary conditions must be applied.

1. The radial displacement at the center of the fiber must be zero; i.e.,

$$u_r(0, z) = 0.0. \tag{36}$$

2. The axial displacement at the spinneret must be zero

$$u_z(r, 0) = 0.0. \tag{37}$$

Both of these conditions are applied by direct substitution into the final set of equations.

Once the displacements have been determined, the stresses in each element may be calculated. By Hooke's law, the stresses are given by

$$\{\sigma\} = [D][B]\{U\} - [D]\{\epsilon_0\} \tag{38}$$

where

$$\{\sigma\} = [\sigma_{rr}\sigma_{zz}\sigma_{\theta\theta}\tau_{rz}]^T. \tag{39}$$

As before, the elements of $[B]$ are variable. Because centroidal and average values were used in calculating the displacements, the stresses should also be calculated at the centroid. Thus $[\overline{B}]$ is substituted for $[B]$ in Eq. (38). Note

that the stresses are now constant within an element, requiring a relatively fine grid of nodes to provide accurate results.

Because centroidal stress values are difficult to interpret, it is preferable to calculate the stresses at the nodes. Segerlind[7] describes such a method for properly distributing element stresses to the nodes. Consistent nodal stresses are found by solving the system of equations

$$[C]\{\sigma^*\} = \{R\} \tag{40}$$

where

$$[C] = \sum_{\substack{\text{all}\\ \text{elements}}} [c^{(e)}] = \sum_{\substack{\text{all}\\ \text{elements}}} \int_V [N]^T [N]\, dV \tag{41}$$

$$\{R\} = \sum_{\substack{\text{all}\\ \text{elements}}} \{r^{(e)}\} = \sum_{\substack{\text{all}\\ \text{elements}}} \int_V \bar{\sigma}[N]^T\, dV \tag{42}$$

and $\{\sigma^*\}$ is the vector of nodal stress values. Here, $\bar{\sigma}$ is the calculated element stress and the calculation is repeated for each of the four stress components. Integration by the area coordinate method[7] yields the following results.

$$[c^{(e)}] = \frac{\pi A}{30}\begin{bmatrix} (6R_i + 2R_j + 2R_k) & (2R_i + 2R_j + R_k) & (2R_i + R_j + 2R_k) \\ (2R_i + 2R_j + R_k) & (2R_i + 6R_j + 2R_k) & (R_i + 2R_j + 2R_k) \\ (2R_i + R_j + 2R_k) & (R_i + 2R_j + 2R_k) & (2R_i + 2R_j + 6R_k) \end{bmatrix} \tag{43}$$

$$\{r^{(e)}\} = \frac{\pi A\bar{\sigma}}{6}\begin{Bmatrix} (2R_i + R_j + R_k) \\ (R_i + 2R_j + R_k) \\ (R_i + R_j + 2R_k) \end{Bmatrix}. \tag{44}$$

RESULTS AND DISCUSSION

The most useful aspect of a model such as this is its ability to predict changes in temperatures and stresses caused by changes in spinning conditions. To this end, a series of simulations was made to determine which spinning

TABLE I
Physical and Mechanical Properties of Polystyrene

ρ	1040.0 kg/m^3
C_p	1836.8 J/kg · K
k	0.128 W/m · K
μ_s	0.32
α_s	5.7×10^{-5} K^{-1}
α_m	1.7×10^{-4} K^{-1}
T_g	373.15 K
A_1	5.1052×10^{-10} Pa · s[a]
B_1	14520.8 K[a]

[a] Elongational viscosity is given by $\beta = 3A_1\exp(B_1/T)$.

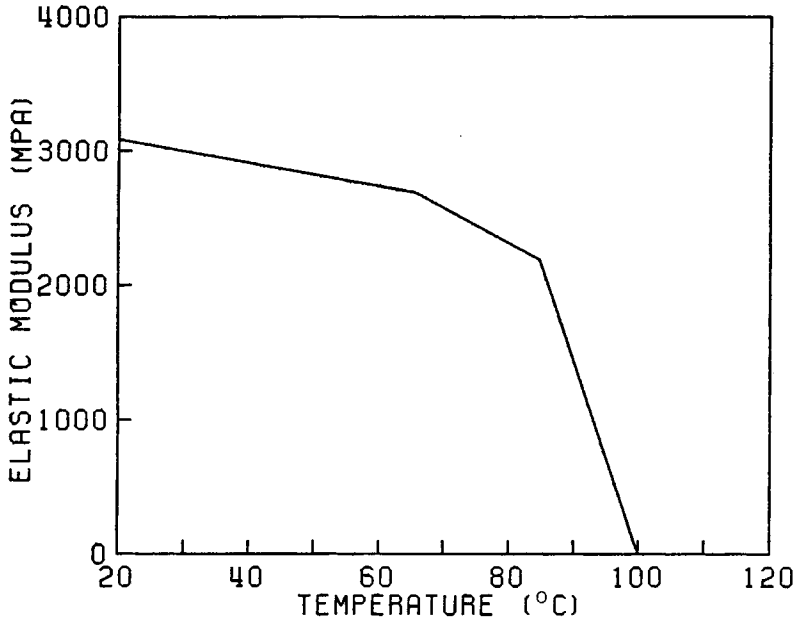

Fig. 3. Elastic modulus data for polystyrene.

TABLE II
Input Data for Simulation Runs

Run number	Spinneret diameter (m) × 10^6	Mass flow rate (kg/s) × 10^6	Cooling air temperature (K)	Spinning temperature (K)	Take-up speed (m/s)
1	688.8	6.053	300.95	538.15	4.4340
2	516.6	6.053	300.95	538.15	4.4340
3	861.0	6.053	300.95	538.15	4.4340
4	688.8	4.540	300.95	538.15	4.4340
5	688.8	8.016	300.95	538.15	4.4340
6	688.8	6.053	280.95	538.15	4.4340
7	688.8	6.053	320.95	538.15	4.4340
8	688.8	6.053	300.95	528.15	4.4340
9	688.8	6.053	300.95	548.15	4.4340
10	688.8	6.053	300.95	538.15	3.3255
11	688.8	6.053	300.95	538.15	5.5425

parameters are most important. Polystyrene was chosen as the material for the simulation. The necessary material properties are given in Table I and Figure 3, while the variations made are listed in Table II.

BASE CASE—RUN 1

Figure 4 shows the fiber radius for Run 1 as predicted by Eqs. (1) and (2). This model gives a solidification length of 0.1798 m, but it should be noted that the drawdown is more than 99% complete at an axial distance of 0.05 m. The spinline tension is calculated as 1.414×10^{-3} N.

Figure 5 shows the surface and center-line temperature profiles as calculated by the finite-element method. The model predicts that solidification

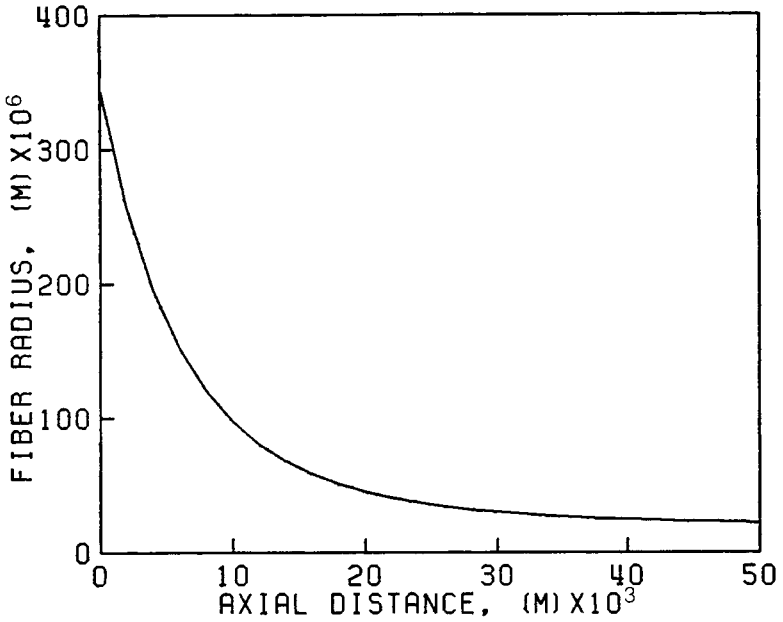

Fig. 4. Predicted fiber radius profile for Run 1.

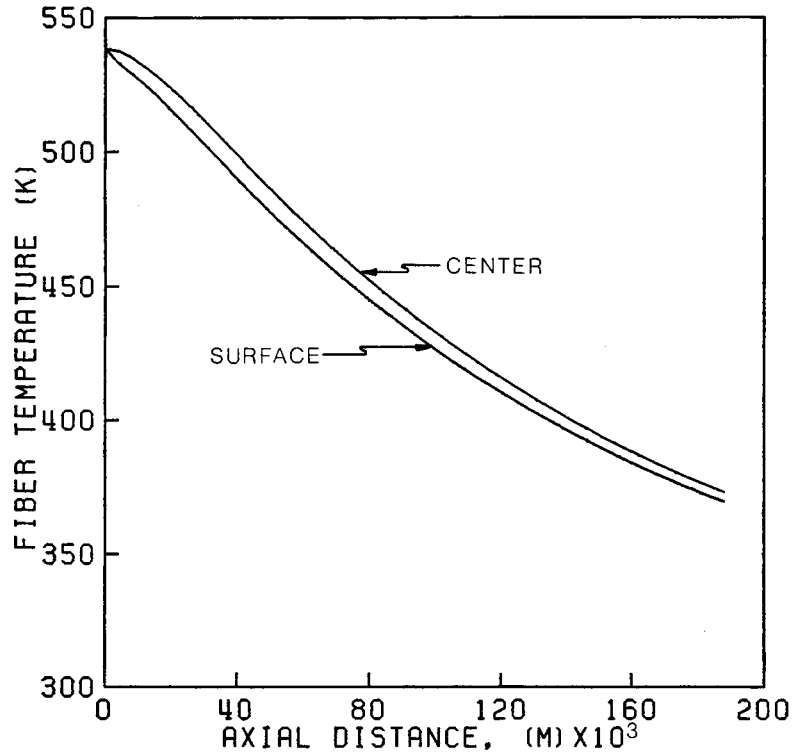

Fig. 5. Temperature profiles for Run 1.

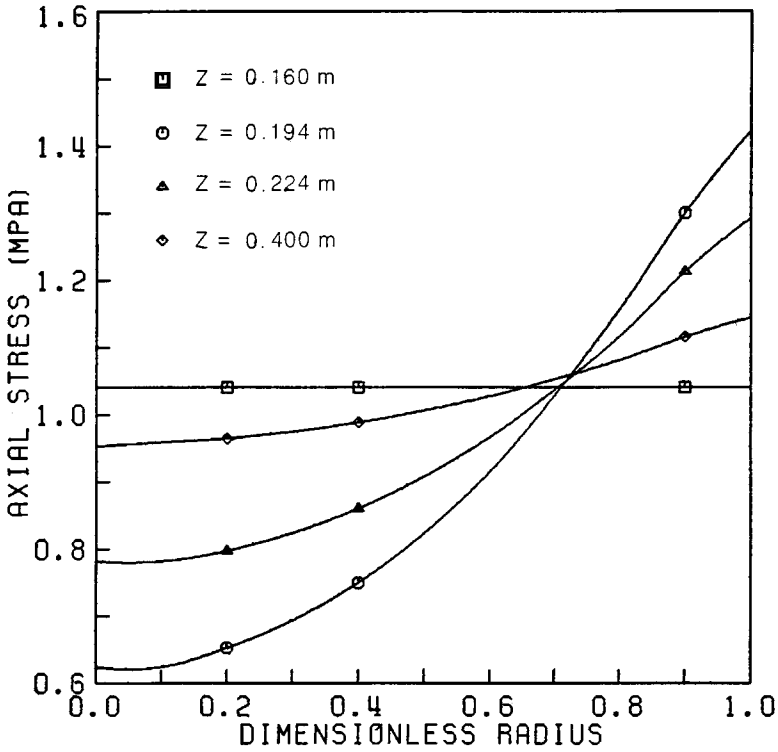

Fig. 6. Axial stress profiles for Run 1.

begins at 0.1803 m, nearly identical to the value found above. However, solidification is not complete until $z = 0.1874$ m, indicating that radial temperature variation is significant. The center-to-surface temperature difference has a maximum value of 8.90 K at $z = 0.038$ m and a value of 3.64 K at the onset of solidification. These differences will affect the magnitude of the thermal stresses within the fiber.

Figure 6 shows the radial variation in normal axial stress at several axial positions. Before solidification ($z = 0.160$ m), the stress profile is very flat, indicating that thermal stresses in the molten region are small compared to the spinline tension. Immediately after solidification ($z = 0.194$ m), significant radial variation in axial stress is observed. This variation is due primarily to the rapid variation of modulus with temperature just below the glass transition. As the fiber cools further, the modulus variation decreases and the stress profiles begin to flatten.

These stress distributions conform to the predictions of Ziabicki.[11] Stresses are larger at the surface because these layers are cooler and have a higher modulus. Thus they can support a greater proportion of the spinline tension than the hot, softer interior. Note that near the center of the fiber, calculated stresses deviate from the smooth curves shown. This is caused by an increase in the error of the $\bar{r}$ approximation in Eqs. (34) and (35) as r approaches zero. Because large increases in memory are required to increase the number of nodes in the radial direction, extrapolation of the data to obtain center-line values is recommended.[12]

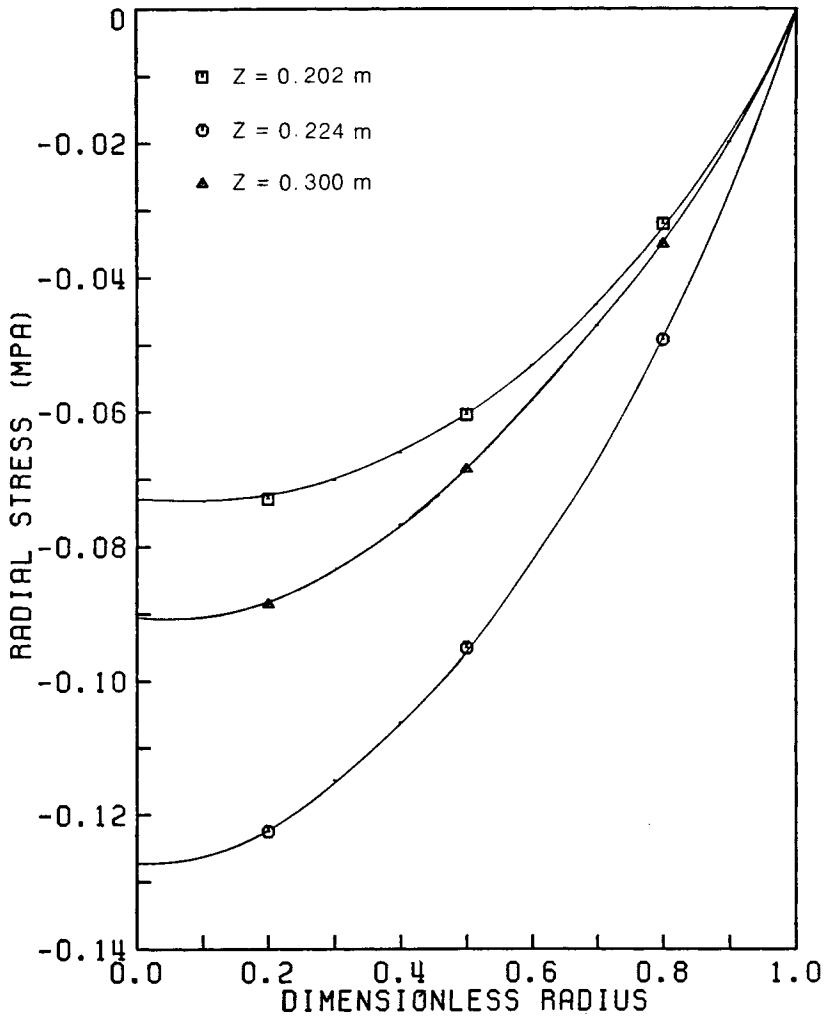

Fig. 7. Radial stress profiles for Run 1.

Figures 7 and 8 show radial and hoop stresses at several points after solidification of the fiber. The center and surface stresses are found to initially increase with z, again due to modulus variation with temperature. However, at $z = 0.224$ m, the stresses reach maxima, indicating a point of potential mechanical failure of the fiber. These stresses decay to zero as the radial temperature gradient decreases.

Although the radial and hoop stresses are somewhat smaller than the axial stress, they may cause problems in the spinning operation. The tensile hoop stress at the surface of the fiber can cause longitudinal cracks to develop in brittle fibers such as glass.[1] Because of the drawing process, preferred orientation is induced in the fibers during spinning, resulting in an anisotropic material. Mechanical strength in the direction normal to the orientation may be considerably less than that in the axial direction. The effects of elevated temperature must also be considered. Thus, the maxima in these stress

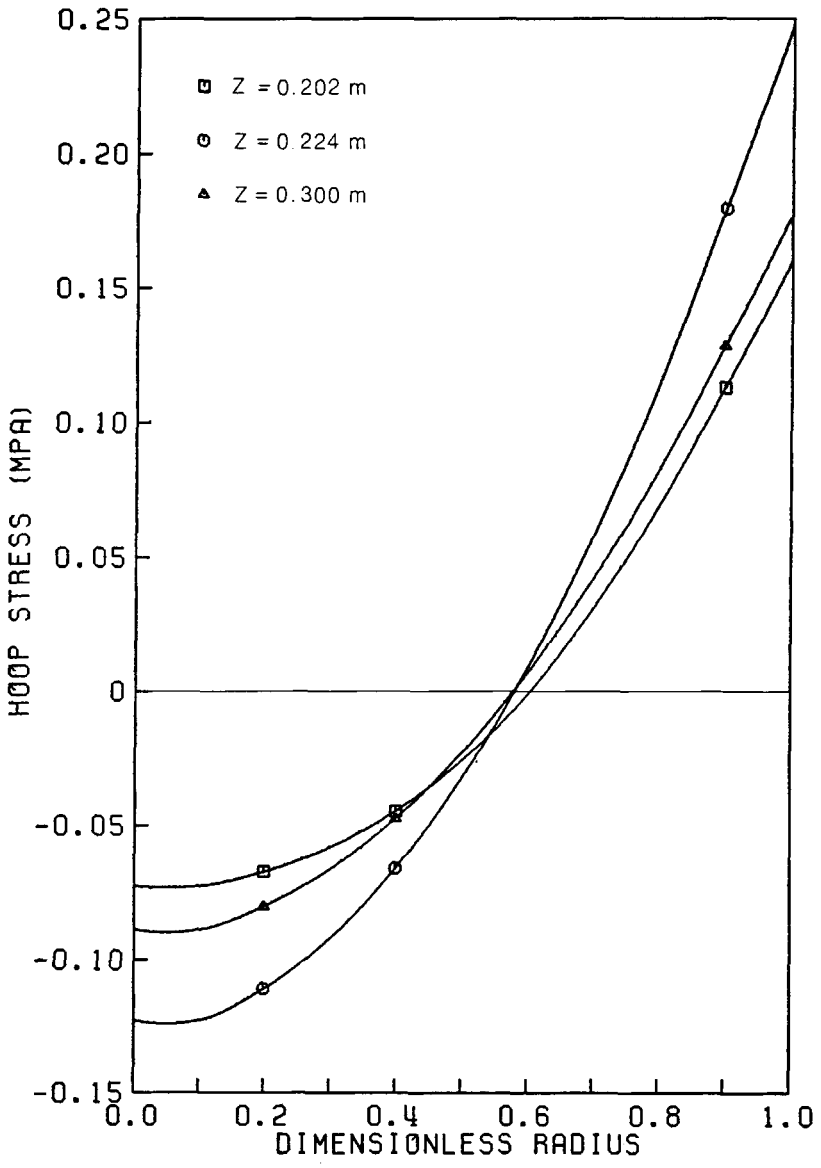

Fig. 8. Hoop stress profiles for Run 1.

components represent potential problems in the spinline for any material with a highly anisotropic breaking strength.

EFFECTS OF SPINNING CONDITIONS

Simulations were made to determine the effects of the spinning conditions on temperature and stress distributions in the spinline, as noted in Table II. Critical results from the simulations are summarized in Table III.

Variations made in Runs 2 and 3 indicate that the only significant effects of the spinneret diameter is on spinline tension. As the initial diameter increases, the draw ratio increases and the required tension must also increase. There is

TABLE III
Summary of Simulation Results

Run number	Variable change	% Change in variable	% Change in max. temp. diff.	% Change in spinline tension	% Change in max. radial stress at center	% Change in max. hoop stress at surface
2	D_{spin}	−25.0	+0.6	−6.4	+0.3	+0.2
3	D_{spin}	+25.0	−0.4	+4.6	+0.3	+0.1
4	W	−25.0	−4.8	−1.8	−4.1	−4.2
5	W	+25.0	+4.0	+1.3	+4.0	+3.7
6	T_a	−6.6	+8.5	+7.5	+34.1	+34.7
7	T_a	+6.6	−8.7	−7.8	−34.4	−34.8
8	T_{spin}	−1.9	−4.4	+65.4	−0.1	−0.3
9	T_{spin}	+1.9	+4.4	−38.5	+0.4	+0.5
10	$V_{z,w}$	−25.0	−4.3	−7.7	−4.3	−4.2
11	$V_{z,w}$	+25.0	+3.5	+6.2	+3.9	+3.7

no significance to the fact that the radial and hoop stresses increase in both runs; these changes are within the numerical error expected in the calculations.

Spinning temperature has similar though more pronounced effects, as shown in Runs 8 and 9. Spinline tension changes significantly with T_{spin} because of the resulting change in the material's elongational viscosity. Moderate changes in radial temperature differences are observed, but these cause little change in the maximum stresses. Thus, though spinning temperature is certainly an important variable in properly running a spinning operation, it has little effect on the radial fiber stress distribution.

Very similar effects are seen for mass flow rate (Runs 4 and 5) and take-up speed (Runs 10 and 11). Mass flow rate has a slightly greater effect on a radial temperature difference, while take-up speed influences spinline tension more significantly. Changes in maximum stresses, however, are nearly identical, though not large. These changes are due primarily to changes in the draw ratio and size of the solidified fiber. The similarity of the results follows from the assumption of constant mass flow rate.

Finally, the cooling air temperature is found to have the largest effect on the stress distribution within the fiber. A 6% change in T_a results in a 34% change in maximum stresses. This result is not entirely unexpected. Cooling air temperature is the only variable which directly influences the cooling process. If T_a is decreased, heat transfer from the fiber to the surroundings becomes more rapid and the resultant thermal stresses must be greater. Thus, as a fiber is cooled more slowly, problems with stress cracking are reduced. This, of course, conflicts with the economic need of producing fibers as rapidly as possible.

SUMMARY

In conclusion, thermal stress analysis of fiber melt spinning indicates that, of all the spinning conditions, ambient air temperature has the greatest effect on internal stresses. Mass flow rate and take-up speed have some effect, but not as large as that of T_a. These results show that slow cooling of the spinline is essential if internal thermal stresses in the melt spun fiber are to be

minimized. Experimental verification of these results will be given in a later publication.

APPENDIX: NOMENCLATURE

A = area of element, m^2
A^* = cross-sectional area of fiber, m^2
b_β = shape function coefficient
c_β = shape function coefficient
C_p = heat capacity, J/kg · K
D_{spin} = spinneret diameter, m
E = elastic modulus, Pa
F = spinline tension, N
h = heat transfer coefficient, $W/m^2 \cdot K$
k = thermal conductivity, W/m · K
k_0 = thermal conductivity of air, W/m · K
$L_{\alpha\beta}$ = length of $\alpha - \beta$ side of element, m
N_β = shape function
p_β = applied stress, Pa
R = fiber radius, m
T = absolute temperature, K
T_a = ambient air temperature, K
T_{spin} = spinning temperature, K
u_β = displacement, m
v_β = velocity, m/s
W = mass flow rate, kg/s
α = linear coefficient of thermal expansion, K^{-1}
β = elongation viscosity, Pa · s
ζ = dimensionless axial distance
θ = dimensionless temperature
μ = Poisson's ratio
ν_0 = kinematic viscosity of air, m^2/s
ξ = dimensionless radius
ρ = density, kg/m^3
σ = normal stress, Pa
τ = shear stress, Pa

References

1. K. Chen, et al., *Polym. Prepr.*, **22**, 212 (1981).
2. A. Ziabicki and H. Kawai, *High-speed Fiber Spinning*, Wiley, New York, 1985.
3. E. H. Andrews, *Br. J. Appl. Phys.*, **10**, 39 (1959).
4. T. Matsuo and S. Kase, *J. Appl. Polym. Sci.*, **20**, 367 (1976).
5. S. Kase and T. Matsuo, *J. Polym. Sci.*, **3**, 2541 (1965).
6. K. W. Hutchenson, D. D. Edie, and D. M. Riggs, *J. Appl. Polym. Sci.*, **27**, 3621 (1984).
7. L. J. Segerlind, *Applied Finite Element Analysis*, Wiley, New York, 1976.
8. W. C. M. Gorissen, *Proc. Int. Congr. Rheol.*, **7**, 522 (1976).
9. R. W. Lewis, and B. R. Bass, *J. Heat Transfer*, **98**, 478 (1976).
10. M. Rigdahl, *Int. J. Polym. Mat.*, **5**, 43 (1976).
11. A. Ziabicki, *Proc. Fiber Prod. Conf.*, 1-1 (1984).
12. E. L. Wilson, *AIAA Journal*, **3**, 2269 (1965).

Received December 20, 1985
Accepted July 2, 1986